physica status solidi

pss

www.pss-journals.com

reprint

WILEY-VCH

Phys. Status Solidi A **213,** No. 4, 1002–1009 (2016) / **DOI** 10.1002/pssa.201532711

physica status solidi a
www.pss-a.com
applications and materials science

Synthesis of wide bandgap Ga_2O_3 ($E_g \sim 4.6$–4.7 eV) thin films on sapphire by low pressure chemical vapor deposition

Subrina Rafique, Lu Han, and Hongping Zhao*

Department of Electrical Engineering and Computer Science, Case Western Reserve University, Cleveland, OH 44106, USA

Received 11 September 2015, revised 25 October 2015, accepted 9 November 2015
Published online 2 December 2015

Keywords Ga_2O_3 thin film, low pressure chemical vapor deposition, wide bandgap

* Corresponding author: e-mail hongping.zhao@case.edu, Phone: +1 2163684120, Fax: +1 2163686888

This paper presents the synthesis of wide bandgap Ga_2O_3 thin films on differently oriented sapphire substrates by using low pressure chemical vapor deposition (LPCVD) technique. The effects of substrate orientation on the Ga_2O_3 thin film surface morphology, crystal orientation, growth rate, and optical properties were studied. The Ga_2O_3 thin films were synthesized on the *c*-plane (0001), *a*-plane (11−20), and *r*-plane (1−102) sapphire substrates using high purity metallic Ga and oxygen (O_2) as source materials and argon (Ar) as carrier gas. The Ga_2O_3 thin films grown on the *c*-plane and *a*-plane sapphire substrates are composed of pure β-Ga_2O_3. A mixture of β-Ga_2O_3 and α-Ga_2O_3 phases is observed for the films grown on *r*-plane sapphire substrate. Well-distinct transmission, absorption, and reflectance edge at $E_g \sim 4.6$–4.7 eV are visible for all the films in the optical spectra measured in the spectral range from 200 to 800 nm.

1 Introduction Group III–VI semiconductor material Ga_2O_3 has attracted much attention due to its excellent chemical and thermal stability up to 1400 °C [1]. In addition, it is a wide bandgap material with direct bandgap of ∼4.9 eV at room temperature [2, 3] and exhibits high transparency in the deep-UV to visible wavelength region. Due to its very wide bandgap, Ga_2O_3 is expected to possess larger breakdown field than GaN ($E_g \sim 3.4$ eV) and SiC ($E_g \sim 3.2$ eV) which are being used in high power electronics nowadays [4]. Unintentionally doped Ga_2O_3 shows n-type conductivity mainly due to oxygen vacancies which act as shallow donors [5]. For a precise control of the doping level in Ga_2O_3 for device applications, both n-type doping [6, 7] and p-type doping [8, 9] have been studied previously. These properties enable the applications of Ga_2O_3 for optical emitters at deep-UV [10, 11], transparent conductors [12], and transparent electronic devices [13]. The excellent thermal stability has also been utilized for fabricating high temperature gas sensors [14, 15]. In addition, Ga_2O_3 thin films have been applied for field effect transistors [4, 16]. Importantly, Ga_2O_3 is a promising candidate for solar blind photodetectors with cut-off wavelength at ∼250 nm [17–19]. These photodetectors have vast military and civil applications such as missile tracking, ozone holes monitoring, and fire detection. Novel nanofunctional devices based on low dimensional Ga_2O_3 nanostructures such as nanowire-based field effect transistors (FETs) [20, 21] and nanophotonics switches [22] have been reported recently. In addition, single crystal β-Ga_2O_3 are being used as substrates for epitaxial growth of GaN layer [23–25].

At present Ga_2O_3 thin films are prepared on different substrates such as sapphire, GaAs, SiC, and MgO by various methods: sol gel [26, 27], spray pyrolysis [28], molecular beam epitaxy (MBE) [29, 30], metal organic chemical vapor deposition (MOCVD) [31, 32], mist chemical vapor deposition (CVD) [33, 34], and pulsed laser deposition (PLD) [35, 36]. However, there are limited studies on the CVD growth of Ga_2O_3 thin films [37, 38]. The crystal structures and properties of the Ga_2O_3 thin films significantly depend on the growth conditions and substrate selections. Five phases of Ga_2O_3 are known so far: α, β, γ, δ, and ε. Grown above 870 °C, β-phase Ga_2O_3 with monoclinic crystal structure is the most stable material [39]. The reported growth rates of Ga_2O_3 thin films are relatively low. For example, some reported growth rates of Ga_2O_3 thin films grown by atmospheric pressure chemical vapor

deposition (APCVD), MBE, MOCVD, and PLD are 2.3 [38], 0.09 [40], 0.44 [41], and 0.22 $\mu m\,h^{-1}$ [42], respectively. It is indispensable to increase the growth rate of Ga_2O_3 films for practical device applications.

In this paper, we studied the synthesis of Ga_2O_3 thin films on differently oriented sapphire substrates using low pressure chemical vapor deposition (LPCVD) technique. The growth rates for the thin films grown on the *c*-plane (0001), *a*-plane (11−20), and *r*-plane (1−102) sapphire substrates are estimated as 1.1, 1.8, and 0.4 $\mu m\,h^{-1}$, respectively. The surface morphology, crystal orientation, and optical properties of the Ga_2O_3 thin films were studied in detail. We found that the Ga_2O_3 thin film grown on the *c*-plane sapphire substrate has the smoothest morphology with single (−201) plane orientation. The thin film grown on the *a*-plane sapphire substrate showed dominant (111) plane orientation and the thin film grown on the *r*-plane sapphire substrate showed the presence of α-phase Ga_2O_3 mixed with β-phase Ga_2O_3.

2 Experimental

2.1 Growth of Ga_2O_3 thin films on sapphire substrates of different orientations A single zone tube furnace with programmable temperature controller was used for the synthesis of the monoclinic β-Ga_2O_3 thin films. *c*-plane (0001), *a*-plane (11−20), and *r*-plane (1−102) sapphire were used as the substrates for the growths. Prior to the CVD growth, the substrates were cleaned with acetone and isopropanol, rinsed by de-ionized water, and dried with nitrogen flow. High purity gallium pellets (Alfa Aesar, 99.99999%) was used as the source material. The source was put in a quartz crucible, which was placed inside a quartz tube of diameter 1″ and length 28″ in such a way that the source was located at the center of the furnace. The substrates were placed horizontally at the downstream of the tube. Then the chamber was pumped down to a base pressure of ∼1 mTorr. Prior to heating up the chamber to the desired growth temperature, the chamber was purged with argon (100 sccm) for 30 min. The chamber was then heated up to 900 °C under the flow of argon. The growth was then carried out at pressure of 1 Torr by flowing 5 sccm of oxygen and 100 sccm of argon. The samples were taken out after cooling down to room temperature under argon flow.

2.2 Material characterization The crystal structure, morphology, crystal orientation and composition of the Ga_2O_3 thin films were characterized by using X-ray diffraction (XRD), field emission scanning electron microscopy (FESEM), and energy dispersive spectroscopy (EDS). XRD spectra were collected on a Rigaku D/Max 2200 with CuK_α radiation (1.54 Å). EDS spectra and FESEM images were taken with the Helios 650. For photoluminescence study, a xenon lamp with an output power of 450 W was used as the excitation source for the emission spectra. The selected excitation wavelength was at 300 nm. The transmission, reflectance, and absorbance spectra were taken with Cary 6000i UV-VIS-NIR spectrophotometer in the spectral range from 188 to 1800 nm. The Raman spectra were taken at room temperature using a linearly polarized laser beam of 532 nm. The beam was focused on the sample by a 100X objective. The laser power and the beam diameter were ∼200 μW and ∼1 μm, respectively.

3 Results and discussions

3.1 Ga_2O_3 thin films grown on sapphire substrates of different orientations Figure 1 shows the top view FESEM images of Ga_2O_3 thin films grown on differently oriented sapphire substrates at 900 °C for 40 min.

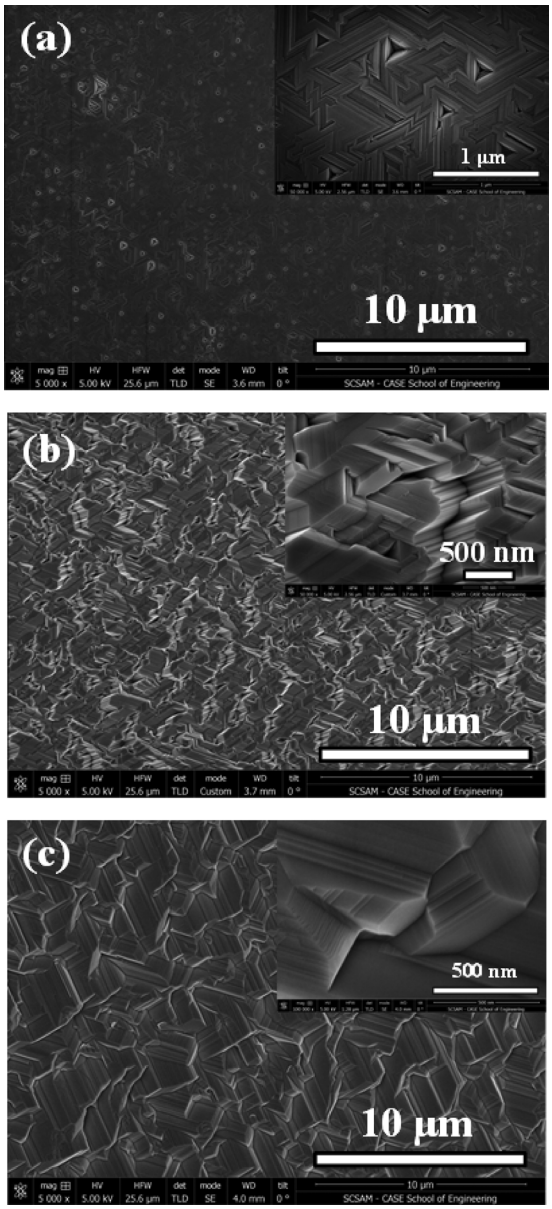

Figure 1 Top view FESEM images of the Ga_2O_3 thin films grown on: (a) *c*-plane (0001) sapphire, (b) *a*-plane (11−20) sapphire, and (c) *r*-plane (1−102) sapphire. Insets show the high magnification top view FESEM images of the Ga_2O_3 thin films.

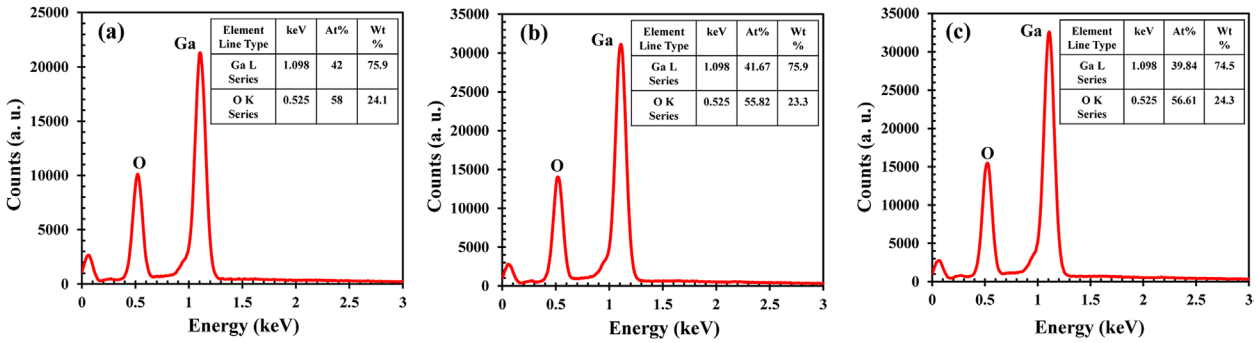

Figure 2 EDS spectra of the Ga_2O_3 thin films grown on: (a) *c*-plane (0001), (b) *a*-plane (11−20), and (c) *r*-plane (1−102) sapphire substrates.

The dependence of the surface morphology of Ga_2O_3 thin films on sapphire substrate orientation is clearly visible in all the images. The Ga_2O_3 film grown on the *c*-plane (0001) sapphire substrate is composed of small pseudo hexagonal domains. The well-defined grain boundaries are clearly visible in the image. The Ga_2O_3 film grown on the *a*-plane (11−20) sapphire substrate is formed by elongated and isometric crystals of different orientations. The Ga_2O_3 film grown on the *r*-plane (1−102) sapphire substrate is also composed of well-oriented isometric crystals. All the SEM images show the representative morphologies of the samples grown on different substrates.

The EDS spectra of the Ga_2O_3 thin films grown on the *c*-, *a*-, and *r*-plane sapphire substrates at 900 °C for 40 min are shown in Fig. 2. Note that EDS has been widely employed as a characterization method to estimate the atomic percentage for Ga_2O_3 materials [43–45]. The atomic percentages of Ga and O for the thin film grown on *c*-plane sapphire substrate are 42 and 58%. For the thin film grown on the *a*-plane sapphire substrate, the atomic percentages are

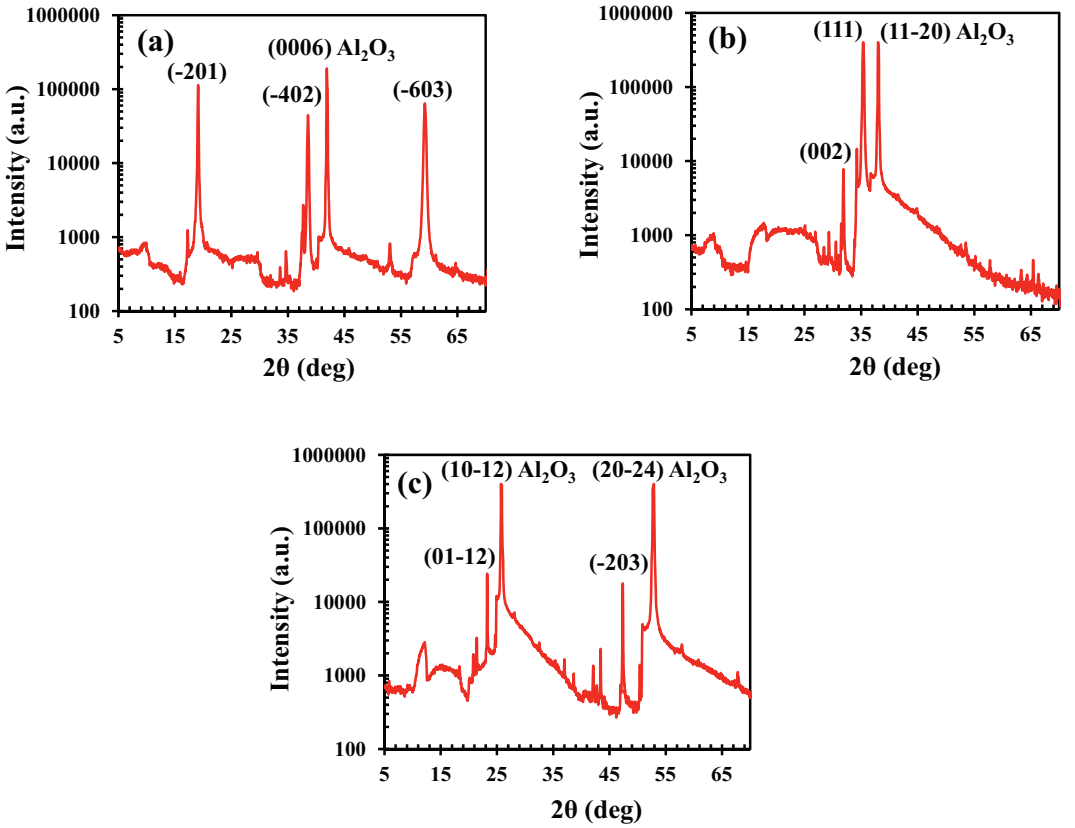

Figure 3 XRD patterns of the Ga_2O_3 thin films grown on (a) *c*-plane (0001), (b) *a*-plane (11−20), and (c) *r*-plane (1−102) sapphire substrates.

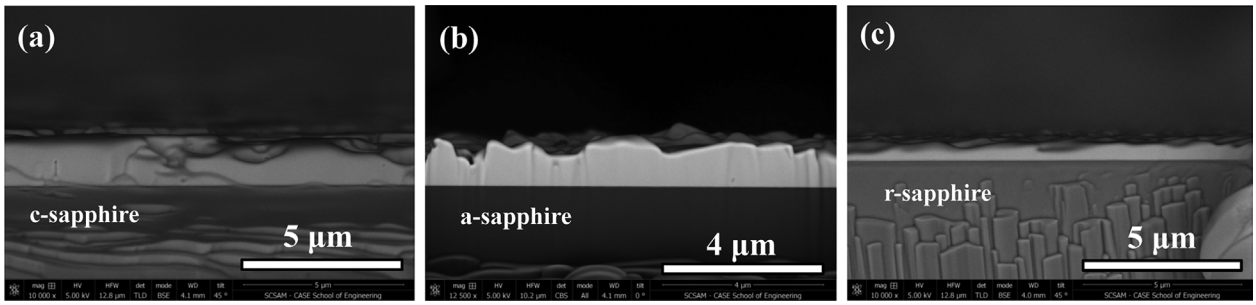

Figure 4 Cross-sectional FESEM images of the Ga_2O_3 thin films grown on differently oriented sapphire substrates: (a) *c*-plane sapphire, (b) *a*-plane sapphire, and (c) *r*-plane sapphire.

41.67 and 55. 82%. In case of the thin film grown on the *r*-plane sapphire substrate, the atomic percentages of Ga and O are 39.84 and 56.61%. The quantitative analysis reveals that for all the three films, the Ga/O atomic ratio is very close to the ideal 2/3. The results revealed that all the Ga_2O_3 films have the stoichiometric chemical composition irrespective of the growth substrates.

The XRD spectra of Ga_2O_3 thin films grown on differently oriented sapphire substrates at 900 °C are shown in Fig. 3. For the thin film grown on the *c*-plane sapphire substrate, all diffraction peaks were indexed as (−201) and higher order diffraction peaks of β-Ga_2O_3. This indicates that (−201) plane is the preferred growth orientation for the thin film grown on *c*-plane sapphire substrate. The film is composed of pure β-Ga_2O_3 with single (−201) plane orientation. This is likely due to the fact that the oxygen atoms of (0001) plane of sapphire substrate has the similar atomic arrangement as the (−201) equivalent plane of β-Ga_2O_3 [46]. This orientation of Ga_2O_3 thin films grown on the *c*-plane sapphire substrate was reported previously grown by gallium evaporation in oxygen plasma and MOVPE [46, 47]. Nakagomi and Kokubun [46] synthesized Ga_2O_3 thin films on *c*-plane and *a*-plane sapphire substrates using metallic gallium as source in oxygen plasma. The substrate temperature and the growth pressure were 600–800 °C and 0.5 mTorr, respectively. From pole figure measurement, they concluded that the [−201] direction of β-Ga_2O_3 is along the [0001] direction of sapphire and (−201) plane of β-Ga_2O_3 is parallel to the surface of *c*-plane sapphire. For the thin film grown on the *a*-plane sapphire substrate, the dominant crystal orientation is (111) plane. Besides this peak, one additional peak appeared at 31.8° which corresponds to (002) plane of β-Ga_2O_3. From the 2θ data of the (002) peak, the lattice parameter *c* is calculated as 5.78 Å which is in good agreement with that of the bulk Ga_2O_3 ($c = 5.8$ Å) [48]. However, the intensity of the (111) peak is ∼50 times higher than that of the (002) peak. Maslov et al. [49] has reported (111) plane-oriented Ga_2O_3 thin film synthesized on the *a*-plane sapphire substrate by sublimation method. Our result differs from Ref. [46] in which they have synthesized (−201) plane-oriented Ga_2O_3 thin film on the *a*-plane sapphire substrate by gallium evaporation in oxygen plasma. For the thin film grown on the *r*-plane sapphire substrate, in addition to the (−203) diffraction peak of β-Ga_2O_3, one additional peak appeared at 23.2° which corresponds to (01−12) diffraction peak of α-Ga_2O_3. Such presence of α-Ga_2O_3 phase in thin film grown on the *r*-plane sapphire substrate by MOVPE was also reported previously [47]. Diffraction peaks corresponding to sapphire substrates are present in all the XRD spectra.

To determine the growth rates of Ga_2O_3 thin films grown on differently oriented sapphire substrates, cross-sectional SEM was performed. The corresponding images are shown in Fig. 4. The films grown on the *c*-plane and *r*-plane sapphire substrates were grown for 90 min at 900 °C. The film thicknesses are estimated as 1.65 and 0.6 µm, respectively. Thus, the growth rates of Ga_2O_3 on *c*-plane and *r*-plane sapphire substrates are estimated as 1.1 and 0.4 µm h^{-1}. On the other hand, the film grown on the *a*-plane sapphire substrate was synthesized at 900 °C for 40 min. The film thickness is 1.2 µm which corresponds to a growth rate of 1.8 µm h^{-1}. We found that the growth rates of the Ga_2O_3 thin films via LPCVD are much higher than those synthesized by MBE, PLD, MOCVD, or mist CVD. The recently reported plasma-assisted MBE grown β-Ga_2O_3 (010) thin film has the highest MBE growth rate of 2.2 nm min^{-1} [50].

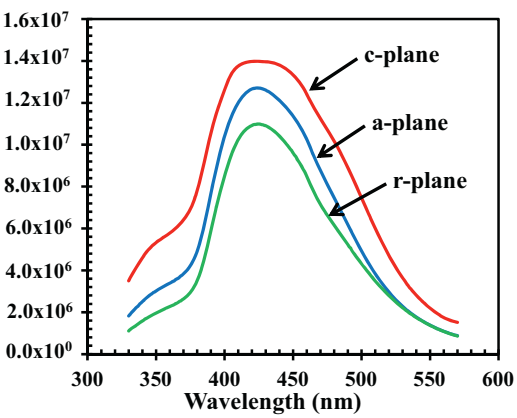

Figure 5 Room temperature PL spectra of the Ga_2O_3 thin films grown on *c*-plane (0001), *a*-plane (11−20), and *r*-plane (1−102) sapphire substrates.

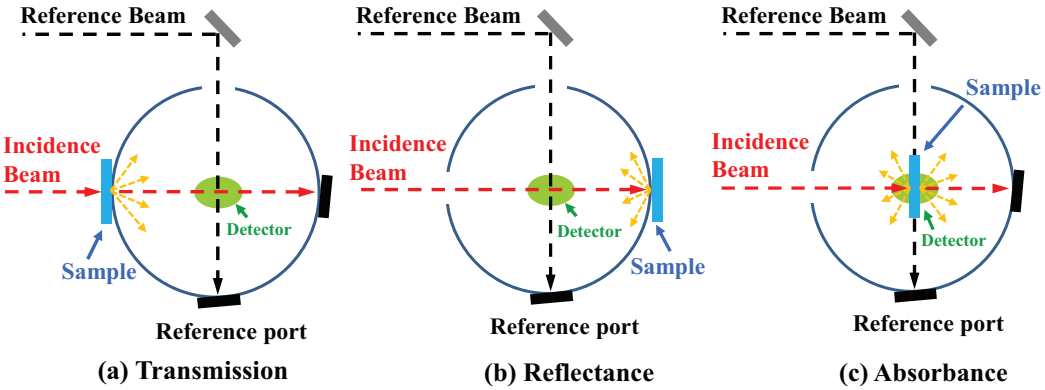

Figure 6 Top view schematics of the optical measurement setup for: (a) transmission, (b) reflectance, and (c) absorbance.

3.2 Optical properties Figure 5 shows the room temperature PL spectra of the Ga_2O_3 thin films grown on differently oriented sapphire substrates. The spectra mainly consist of a strong blue emission broad band at ~420 nm (2.95 eV). A shoulder peak at ~343 nm (3.62 eV) corresponding to the UV emission is also present in all three spectra. The UV emission peak likely originated from the recombination of self-trapped excitons, as predicted from previous studies [51–53]. These excitons are created when an electron at the donor level (formed by oxygen vacancies) recombines with a hole at the acceptor level (formed by either gallium vacancy (V_{Ga}) or gallium–oxygen vacancy pair (V_O–V_{Ga})) [51–53]. The blue emission is originated from the recombination of a donor–acceptor pair (DAP) through tunneling [51, 54–57]. In this study, the Ga_2O_3 thin films were synthesized at a relatively high temperature of

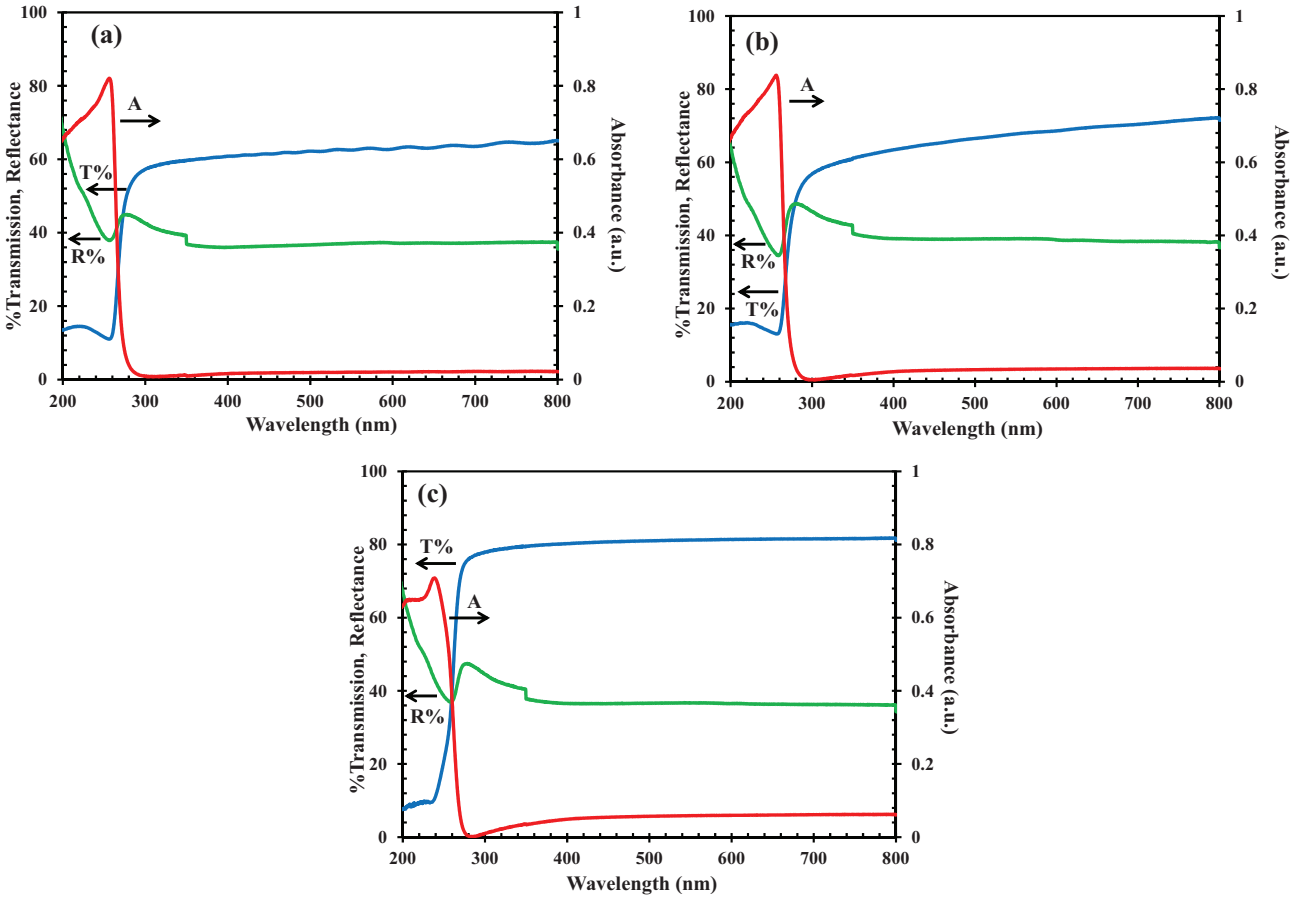

Figure 7 Transmission (T), reflectance (R) and absorbance (A) spectra of the Ga_2O_3 thin films grown on sapphire substrates of different orientations: (a) *c*-plane (0001), (b) *a*-plane (11−20), and (c) *r*-plane (1−102).

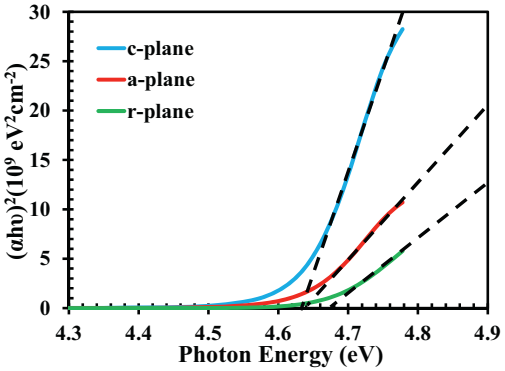

Figure 8 Tauc plot of the as-grown Ga_2O_3 thin films grown on *c*-plane (0001), *a*-plane (11−20), and *r*-plane (1−102) sapphire substrates.

900 °C, thus it is likely that V_{Ga} or V_O–V_{Ga} are formed during the material synthesis.

To estimate the optical bandgap of the Ga_2O_3 thin films grown on the *c*-, *a*-, and *r*-plane sapphire substrates, the transmission, reflectance, and absorbance measurements were conducted. The optical properties were characterized by using Cary 6000i UV-VIS-NIR spectrophotometer in the broad wavelength range from 188 to 1800 nm at an 8° angle of incidence. Figure 6 shows the schematics of the top view measurement set up for (a) transmission, (b) reflectance, and (c) absorbance, collected into an integrating sphere. By loading the samples in the transmission port or reflectance port as shown in Fig. 6(a) and (b), the integrating sphere collects the transmitted or reflected signals and then calibrates them with the reference signal. For the absorbance measurement, the samples were loaded at the center of the integrating sphere as shown in Fig. 6(c).

The measured spectra are shown in Fig. 7. All the films exhibit high optical transmittance (∼60% for Ga_2O_3 on *c*-sapphire, ∼70% for Ga_2O_3 on *a*-sapphire, and ∼80% for Ga_2O_3 on *r*-sapphire) in the near UV and visible wavelength region. We observe an abrupt change in the slope of the transmission and absorption spectra at the bandgap energy for all the films. The estimated optical bandgaps from the Tauc plot (Fig. 8) are E_g (*c*-plane) = 4.64 eV, E_g (*a*-plane) = 4.64 eV, and E_g (*r*-plane) = 4.68 eV. The bandgap energies for all the films are within the range of 4.2–4.9 eV reported previously [58, 59]. The surface reflectance measurements show the consistent results with the distinct reflectance edges occurring at 255–265 nm for the films grown on the *c*-plane, *a*-plane, and *r*-plane sapphire substrates. The clear interference fringes in the visible wavelength for the film grown on the *c*-plane sapphire are an indication of a relative smooth surface.

Room temperature Raman spectra of the Ga_2O_3 thin films grown on *c*-plane (0001), *a*-plane (11−20), and *r*-plane (1−102) sapphire substrates are shown in Fig. 9. The

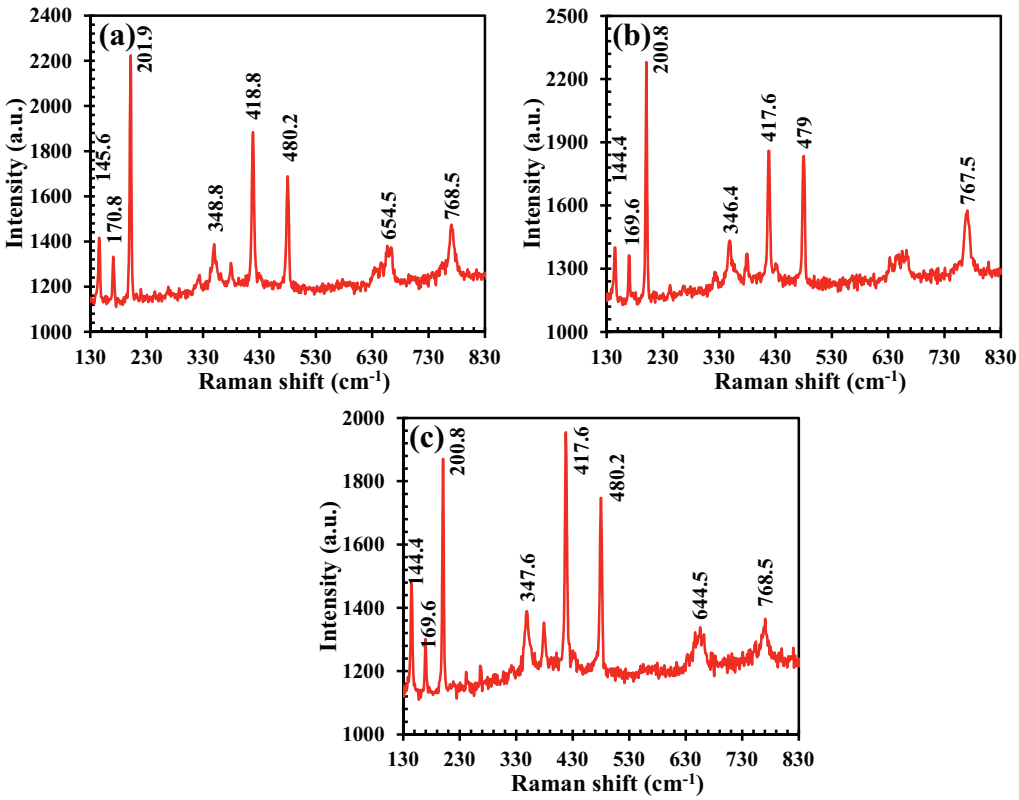

Figure 9 Micro Raman spectra of the as-grown Ga_2O_3 thin films grown on sapphire substrates of different orientations with: (a) *c*-plane (0001), (b) *a*-plane (11−20), and (c) *r*-plane (1−102).

Raman active modes in Ga_2O_3 are classified into three categories: low ($200\,cm^{-1}$), mid ($\sim$480–$310\,cm^{-1}$), and high ($\sim$770–$500\,cm^{-1}$) frequency modes [1]. The low frequency modes are associated with the translation and liberation of tetrahedra–octahedra chains. The mid frequency modes are assigned to the deformation of Ga_2O_6 octahedra. The high frequency modes are associated with the bending and stretching of GaO_4 tetrahedra. For the thin film grown on *c*-plane (0001) sapphire substrate, the peaks are blueshifted by 0.5–$8.2\,cm^{-1}$ compared to the bulk Raman peaks [60]. In case of the thin film grown on *a*-plane (11−20) sapphire substrate, the peaks are blueshifted by 0.4–$7\,cm^{-1}$. For the film grown on *r*-plane (1−102) sapphire substrate, the peaks are blueshifted by 0.4–$8.2\,cm^{-1}$. The Raman peak shift of the grown Ga_2O_3 thin films ranging within 0.4–$8.2\,cm^{-1}$ in comparison to that of the bulk Ga_2O_3 powder is very small.

4 Conclusions In summary, we have synthesized and compared the Ga_2O_3 thin films on sapphire substrates of different orientations using LPCVD technique. EDS analysis indicates that the chemical composition of all the films correspond to stoichiometric Ga_2O_3 independent of the growth substrate. XRD measurements show that the film formed on the *c*-plane sapphire substrate is pure monoclinic β-Ga_2O_3 with single (−201) plane orientation. On the other hand, the thin film grown on the *a*-plane sapphire substrate is composed of β-Ga_2O_3 phase exhibiting dominant (111) plane orientation. For the thin film grown on the *r*-plane sapphire substrate, the presence of α-phase mixed with β-phase Ga_2O_3 was observed. Room temperature PL measurement revealed the presence of two emission bands with their peaks at $\sim$343 and $\sim$420 nm. Optical transmission, reflectance, and absorption spectra consistently indicated the bandgaps of all the Ga_2O_3 films range between 4.6 and 4.7 eV.

Acknowledgements The authors acknowledge financial support through start-up funds from Case Western Reserve University (CWRU). Part of the material characterizations were performed at the Swagelok Center for Surface Analysis of Materials (SCSAM) at CWRU. The optical transmission, reflectance and absorption measurements were performed at the CWRU Solar Durability and Lifetime Extension (SDLE) Center. The Raman spectra measurements were performed at Dr. P. Feng's laboratory at CWRU.

References

[1] S. Kumar, C. Tessarek, G. Sarau, S. Christiansen, and R. Singh, Adv. Eng. Mater. **17**, 709 (2015).
[2] S. Kumar and R. Singh, Phys. Status Solidi RRL **7**, 781 (2013).
[3] H. Murakami, K. Nomura, K. Goto, K. Sasaki, K. Kawara, Q. T. Thieu, R. togashi, Y. Kumagai, M. Higashiwaki, A. Kuramata, S. Yamakoshi, B. Monemar, and A. Koukitu, Appl. Phys. Express **8**, 015503 (2015).
[4] M. Higashiwaki, K. Sasaki, A. Kuramata, T. Masui, and S. Yamakoshi, Appl. Phys. Lett. **100**, 013504 (2012).
[5] M. R. Lorenz, J. F. Woods, and R. J. Gambino, J. Phys. Chem. Solids **28**, 403 (1967).
[6] S. Muller, H. V. Wenckstern, D. Splith, F. Schmidt, and M. Grundmann, Phys. Status Solidi A **211**, 34 (2014).
[7] X. Du, Z. Li, C. Luan, W. Wang, M. Wang, X. Feng, H. Xiao, and J. Ma, J. Mater. Sci. **50**, 3252 (2015).
[8] N. K. Shrestha, K. Lee, R. Kirchgeorg, R. Hahn, and P. Schmuki, Electrochem. Commun. **35**, 112 (2013).
[9] L. L. Liu, M. K. Li, D. Q. Yu, J. Zhang, H. Zhang, C. Qian, and Z. Yang, Appl. Phys. A **98**, 831 (2010).
[10] D. D. Edwards, T. O. Mason, F. Goutenoire, and K. R. Poeppelmeier, Appl. Phys. Lett. **70**, 1706 (1997).
[11] F. K. Shan, G. X. Liu, W. J. Lee, G. H. Lee, I. S. Kim, and B. C. Shin, Appl. Phys. Lett. **98**, 023504 (2005).
[12] N. Ueda, H. Hosono, R. Waseda, and H. Kawazoe, Appl. Phys. Lett. **70**, 3561 (1997).
[13] K. Matsuzaki, H. Yanagi, T. Kamiya, H. Hiramatsu, K. Nomura, M. Hirano, and H. Hosono, Appl. Phys. Lett. **88**, 092106 (2006).
[14] M. Fleischer, S. Kornely, T. Weh, J. Frank, and H. Meixner, Sens. Actuators B **69**, 205 (2000).
[15] M. Ogita, N. Saika, Y. Nakanishi, and Y. Hatanaka, Appl. Surf. Sci. **142**, 188 (1999).
[16] M. Higashiwaki, K. Sasaki, T. Kamimura, M. H. Wong, D. Krishnamurthy, A. Kuramata, T. Masui, and S. Yamakoshi, Appl. Phys. Lett. **103**, 123511 (2013).
[17] Y. Li, T. Tokizono, M. Liao, M. Zhong, Y. Koide, I. Yamada, and J. J. Delaunay, Adv. Funct. Mater. **20**, 3972 (2010).
[18] R. Zou, Z. Zhang, Q. Liu, J. Hu, L. Sang, M. Liao, and W. Zhang, Small **10**, 1848 (2014).
[19] W. Feng, X. Wang, J. Zhang, L. Wang, W. Zheng, P. Hu, W. Cao, and B. Yang, J. Mater. Chem. C **2**, 3254 (2014).
[20] P. C. Chang, Z. Fan, W. Y. Tseng, A. Rajagopal, and J. G. Lu, Appl. Phys. Lett. **87**, 222102 (2005).
[21] Y. Huang, S. Yue, Z. Wang, Q. Wang, C. Shi, Z. Xu, X. D. Bai, C. Tang, and C. Gu, J. Phys. Chem. B **110**, 796 (2006).
[22] C. H. Hsieh, L. J. Chou, G. R. Lin, Y. Bando, and D. Golberg, Nano Lett. **8**, 3081 (2008).
[23] K. Shimamura, E. G. Villora, K. Domen, K. Yui, K. Aoki, and N. Ichinose, Jpn. J. Appl. Phys. **44**, L7 (2005).
[24] S. Ohira, N. Suzuki, H. Minami, K. Takahashi, T. Araki, and Y. Nanishi, Phys. Status Solidi C **4**, 2306 (2007).
[25] E. G. Villora, K. Shimamura, K. Aoki, and K. Kitamura, Thin Solid Films **500**, 209 (2006).
[26] Y. Kokubun, K. Miura, F. Endo, and S. Nakagomi, Appl. Phys. Lett. **90**, 031912 (2007).
[27] Y. Li, A. Trinchi, W. Wlodarski, K. Galatsis, and K. K. Zadeh, Sens. Actuators B **93**, 431 (2003).
[28] H. G. Kim and W. T. Kim, J. Appl. Phys. **62**, 2000 (1987).
[29] E. G. Villora, K. Shimamura, K. Kitamura, and K. Aoki, Appl. Phys. Lett. **88**, 031105 (2006).
[30] K. Sasaki, A. Kuramata, T. Masui, E. G. Villora, K. Shimamura, and S. Yamakoshi, Appl. Phys. Express **5**, 035502 (2012).
[31] N. H. Kim, H. W. Kim, C. Seoul, and C. Lee, Mater. Sci. Eng. B **111**, 131 (2004).
[32] H. W. Kim and N. H. Kim, Mater. Sci. Eng. B **110**, 34 (2004).
[33] D. Shinohara and S. Fujita, Jpn. J. Appl. Phys. **47**, 7311 (2008).
[34] K. Akaiwa and S. Fujita, Jpn. J. Appl. Phys. **51**, 070203 (2012).

[35] M. Orita, H. Ohta, M. Hirano, and H. Hosono, Appl. Phys. Lett. **77**, 4166 (2000).
[36] M. Orita, H. Hiramatsu, H. Ohta, M. Hirano, and H. Hosono, Thin Solid Films **411**, 134 (2002).
[37] E. Auer, A. Lugstein, S. Loffler, Y. J. Hyun, W. Brezna, E. Bertagnolli, and P. Pongratz, Nanotechnology **20**, 434017 (2009).
[38] T. Terasako, H. Ichinotani, and M. Yagi, Phys. Status Solidi C **12**, 985 (2015).
[39] S. Geller, J. Chem. Phys. **33**, 676 (1960).
[40] T. Oshima, T. Okuno, and S. Fujita, Jpn. J. Appl. Phys. **46**, 7217 (2007).
[41] N. M. Sbrockey, T. Salagaj, E. Coleman, G. S. Tompa, Y. Moon, and M. S. Kim, J. Electron. Mater. **44**, 1357 (2015).
[42] F. B. Zhang, K. Saito, T. Tanaka, M. Nishio, and Q. X. Guo, J. Cryst. Growth **387**, 96 (2014).
[43] S. Ohira, T. Sugawara, K. Nakajima, and T. Shishido, J. Alloys Compd. **402**, 204 (2005).
[44] X. Xiang, C. B. Cao, and H. S. Zhu, J. Cryst. Growth **279**, 122 (2005).
[45] K. Girija, S. Thirumalairajan, A. K. Patra, D. Mangalaraj, N. Ponpandian, and C. Viswanathan, Curr. Appl. Phys. **13**, 652 (2013).
[46] S. Nakagomi and Y. Kokubun, J. Cryst. Growth **349**, 12 (2012).
[47] V. Gottschalch, K. Mergenthaler, G. Wagner, J. Bauer, H. Paetzelt, C. Sturm, and U. Teschner, Phys. Status Solidi A **206**, 243 (2009).
[48] H. He, M. A. Blanco, and R. Pandey, Appl. Phys. Lett. **88**, 261904 (2006).
[49] V. N. Maslov, V. I. Nikolaev, V. M. Krymov, V. E. Bugrov, and A. E. Romanov, Phys. Solid State **57**, 1342 (2015).
[50] H. Okumura, M. Kita, K. Sasaki, A. Kuramata, M. Higashiwaki, and J. S. Speck, Appl. Phys. Express **7**, 095501 (2014).
[51] S. Kumar, V. Kumar, T. Singh, A. Hahnel, and R. Singh, J. Nanopart. Res. **16**, 2189 (2014).
[52] J. B. Varley, A. Janotti, C. Franchini, and C. G. Van de Walle, Phys. Rev. B **85**, 081109 (2012).
[53] T. Harwig and F. Kellendonk, J. Solid State Chem. **24**, 255 (1978).
[54] L. Binet and D. Gourier, J. Phys. Chem. Solids **59**, 1241 (1998).
[55] N. M. Ghazali, M. R. Mahmood, K. Yasui, and A. M. Hashim, Nanoscale Res. Lett. **9**, 120 (2014).
[56] P. Guha, S. Chakrabarti, and S. Chaudhuri, Physica E **23**, 81 (2004).
[57] E. G. Villora, M. Yamaga, T. Inoue, S. Yabasi, Y. Masui, T. Sugawara, and T. Fukuda, Jpn. J. Appl. Phys. **41**, L622 (2002).
[58] H. H. Tippins, Phys. Rev. **140**, A316 (1965).
[59] N. Ueda, H. Hosono, R. Waseda, and H. Kawazoe, Appl. Phys. Lett. **71**, 933 (1997).
[60] R. Rao, A. M. Rao, B. Xu, J. Dong, S. Sharma, and M. K. Sunkara, J. Appl. Phys. **98**, 094312 (2005).